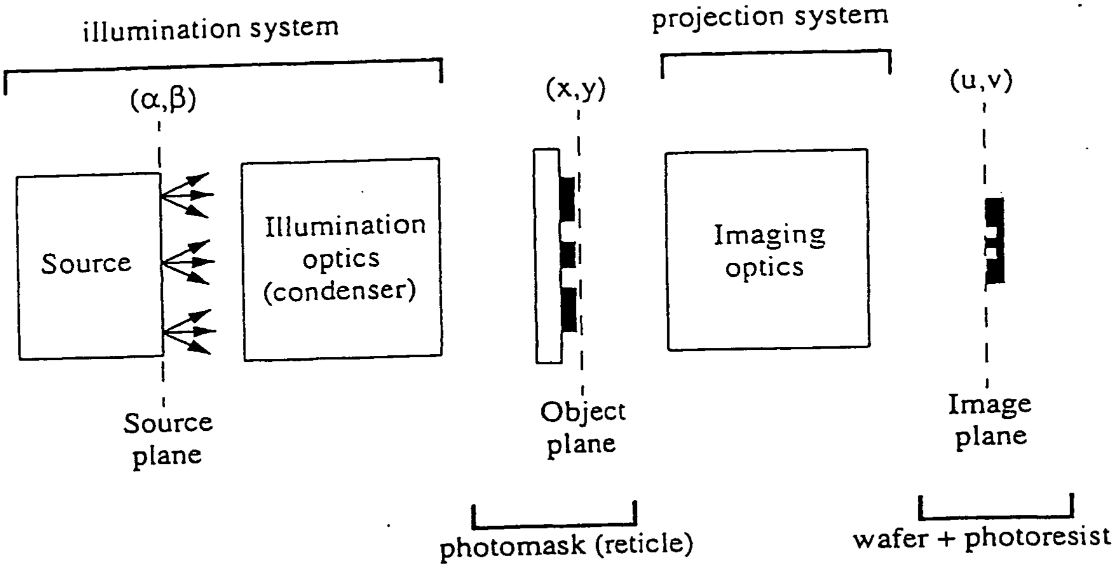

Figure 1. General diagram of an optical photolithography tool

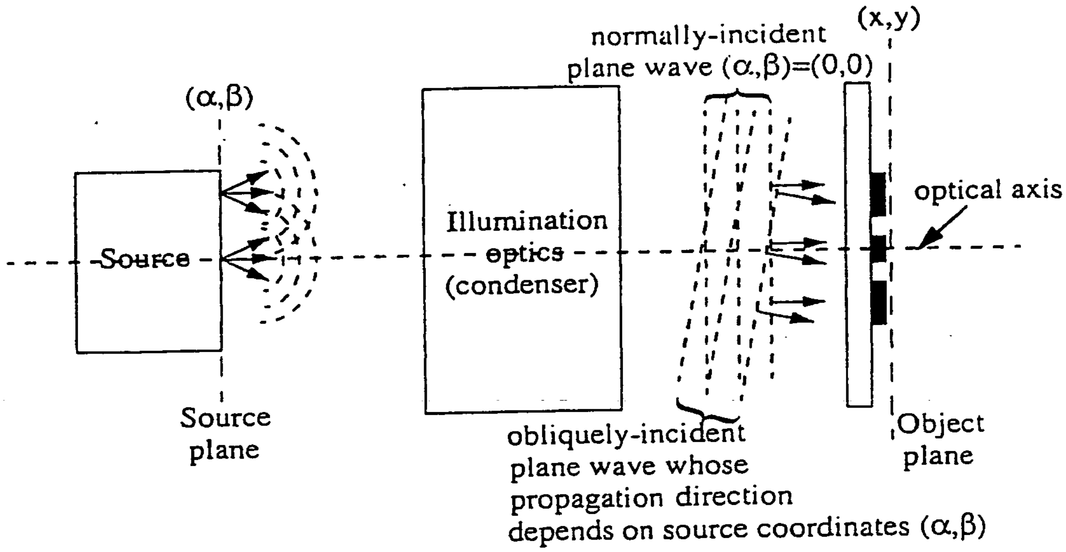
(x,y)
normally-incident plane wave (α,β)=(0,0)
(α,β)
optical axis
~~Source~~
Illumination ~~optics~~ (condenser)
Source plane
obliquely-incident plane wave whose propagation direction depends on source coordinates (α,β)
Object plane

Figure 2A. Illumination with Köhler's method

Each source point emits a spherical wave that is converted by the illumination system into a plane wave incident on the object (photomask). The angle of incidence of the plane wave depends on the location of the source point (α,β) with respect to the optical axis (0,0).

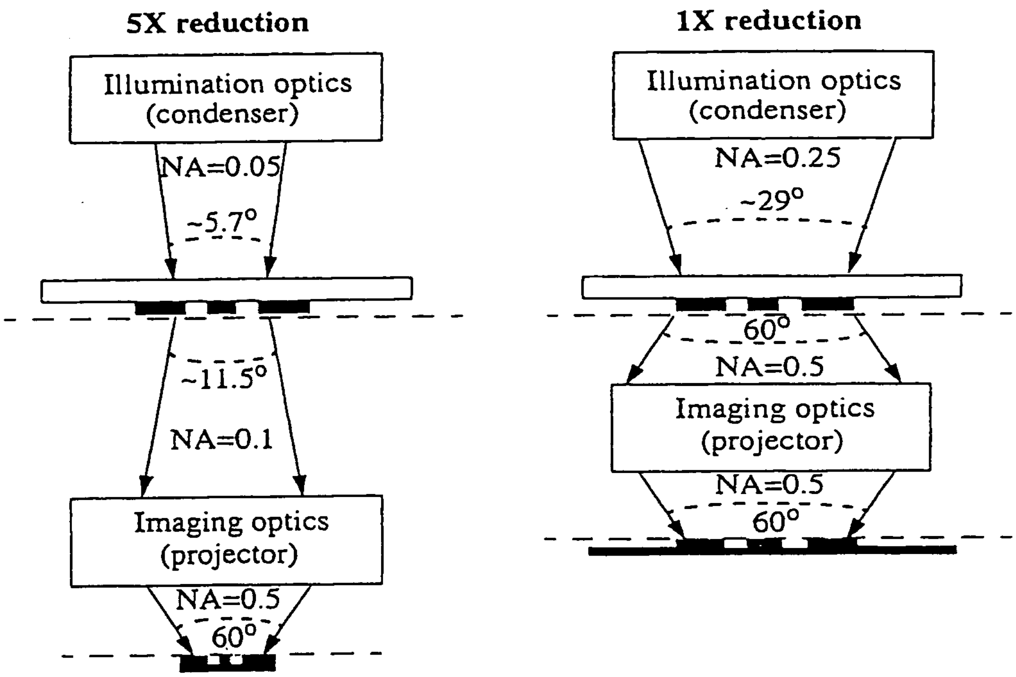

Figure 2B. Numerical apertures and corresponding light acceptance cones of illumination and projection lenses for NA=0.5, $\sigma=0.5$ at 5X and 1X reduction

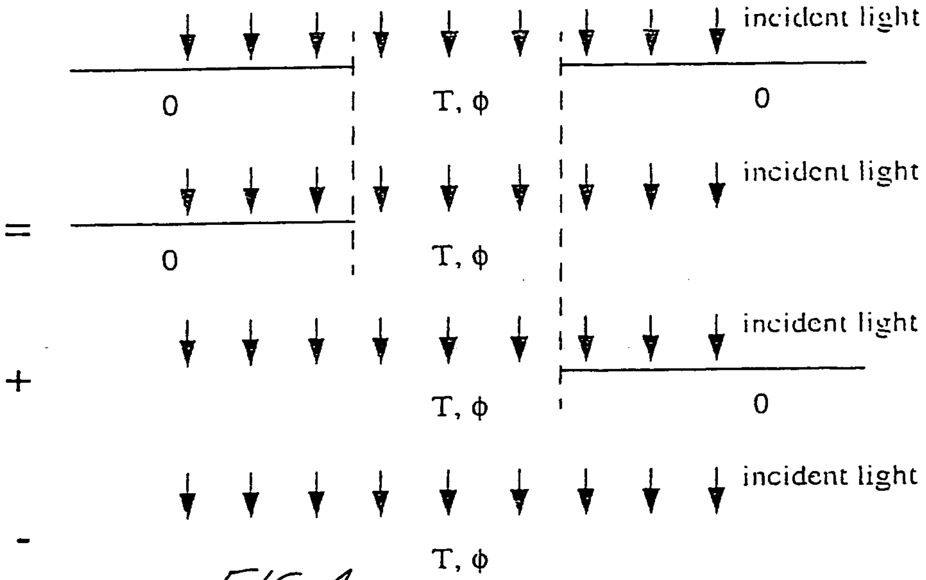

FIG. 4

Decomposition of an opening into two edges

An opening with transmission T and phase φ in an infinitely thin, opaque screen can be decomposed by way of the linearity of the Kirchhoff-Fresnel diffraction integral into two edges. The uniform plane wave illumination is subtracted to restore the light level everywhere.

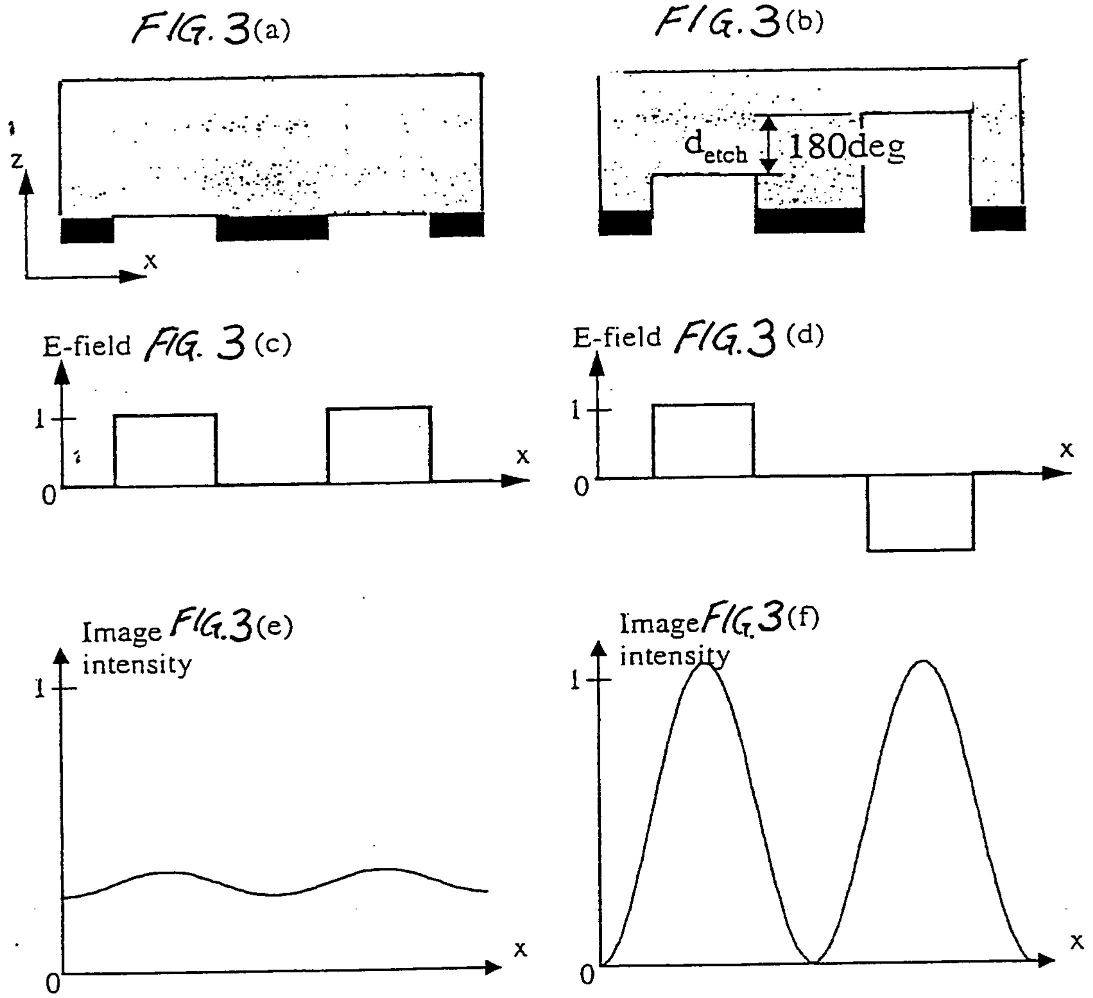

Figure 3 Comparison of operation principles of an alternating phase shift mask (alt. PSM) and a binary (COG) mask

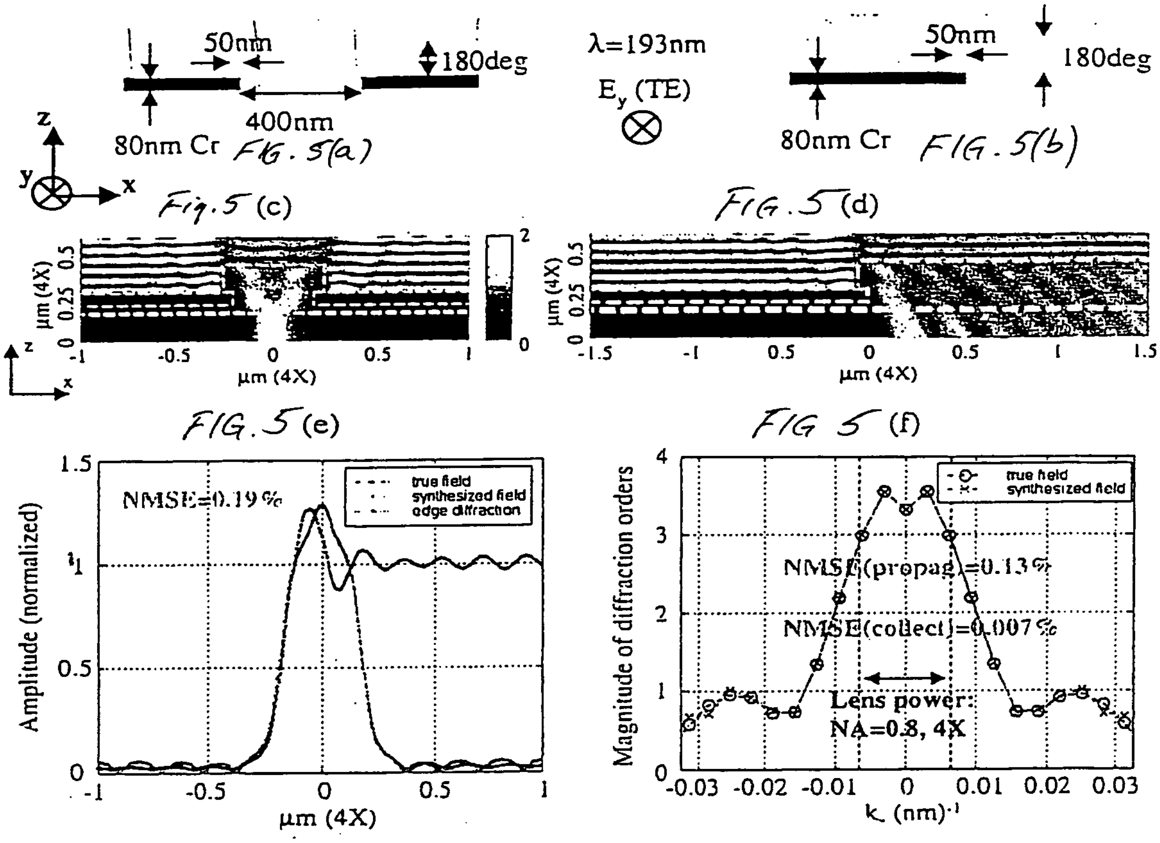
FIG. 5(a) FIG. 5(b) Fig. 5 (c) FIG. 5 (d) FIG. 5 (e) FIG 5 (f)

FIG. 5 Edge-DDM applied on an isolated space

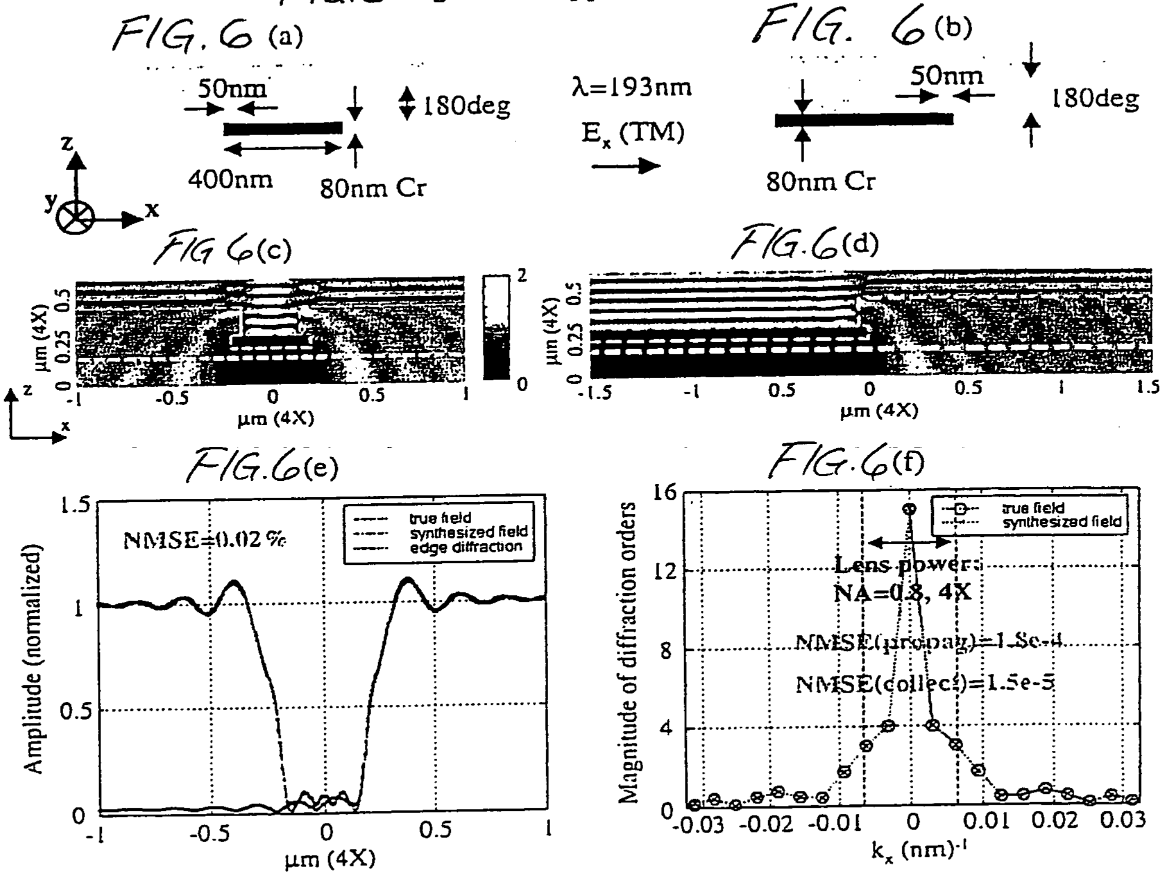
FIG. 6 (a) FIG. 6 (b) FIG 6(c) FIG. 6(d) FIG. 6(e) FIG. 6(f)

FIG. 6 Edge-DDM applied on an isolated line

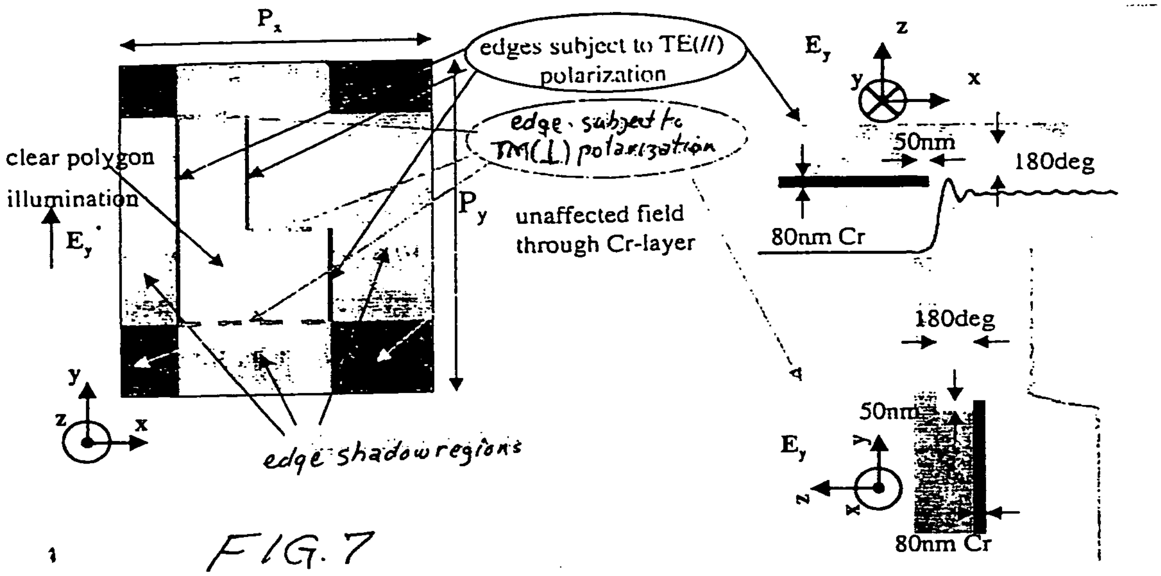

P_x
edges subject to TE(//) polarization
edge subject to TM(⊥) polarization
clear polygon illumination
E_y
P_y
unaffected field through Cr-layer
edge shadow regions
y
z
x
E_y
50nm
180deg
80nm Cr
180deg
50nm
E_y
y
z
x
80nm Cr

FIG. 7

Edge-DDM applied on an arbitrary Manhattan-type polygon

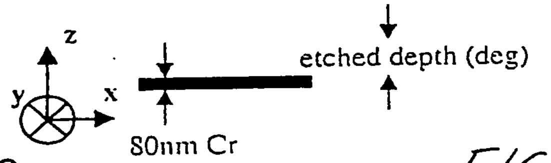

FIG. 8(a)

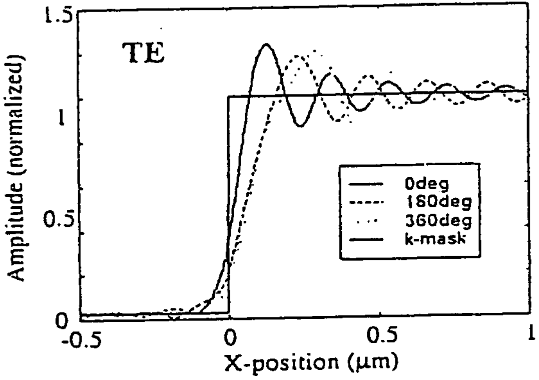

FIG. 8(b)

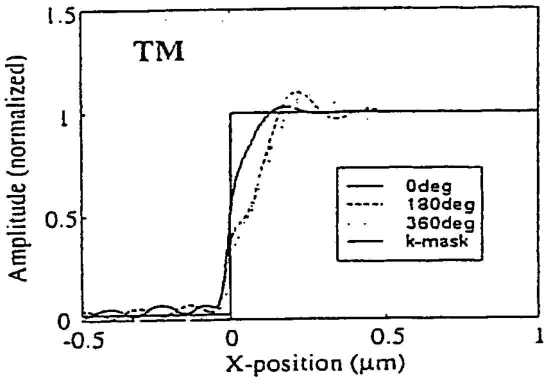

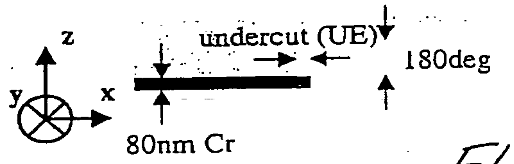

FIG. 8(c)

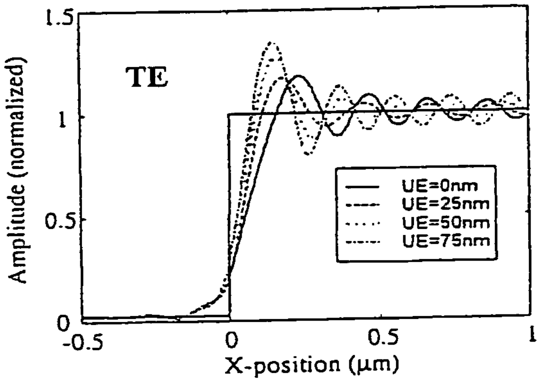

FIG. 8(d)

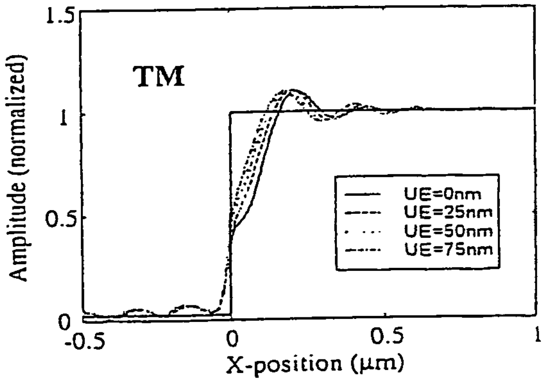

FIG. 9 (a)

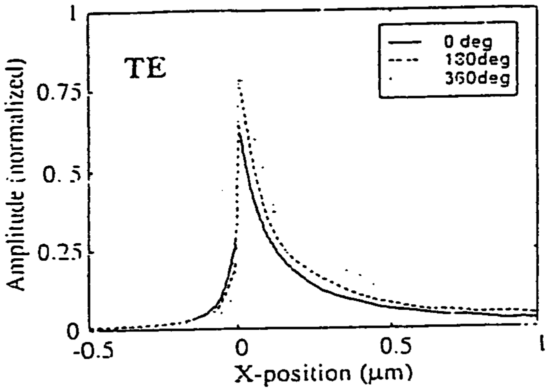

FIG. 9 (b)

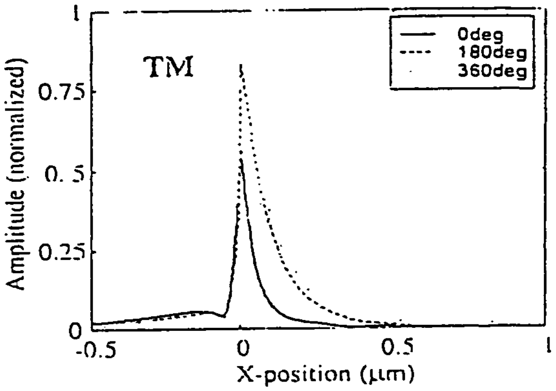

FIG. 9 (c)

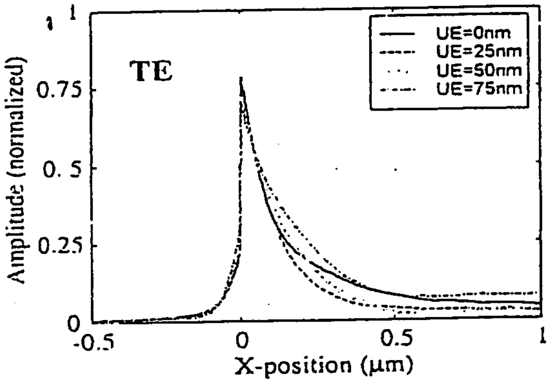

FIG. 9 (d)

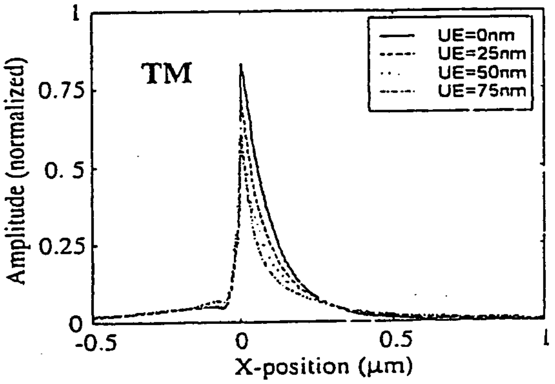

FIG. 10 (a)

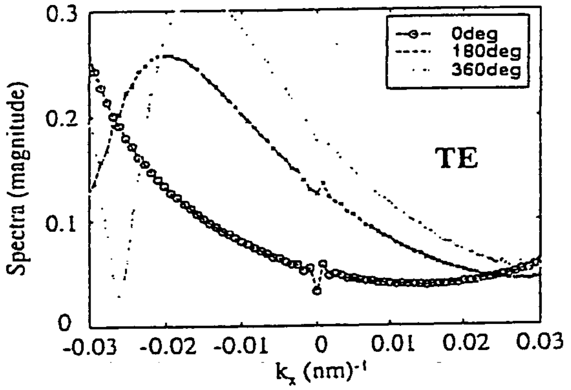

FIG. 10 (b)

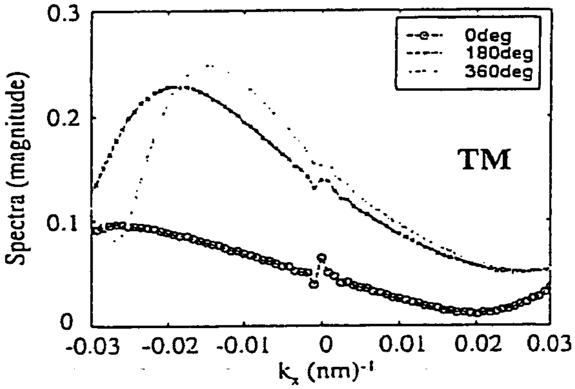

FIG. 10 (c)

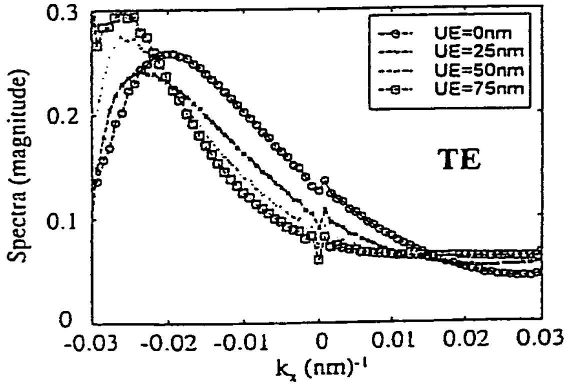

FIG. 10 (d)

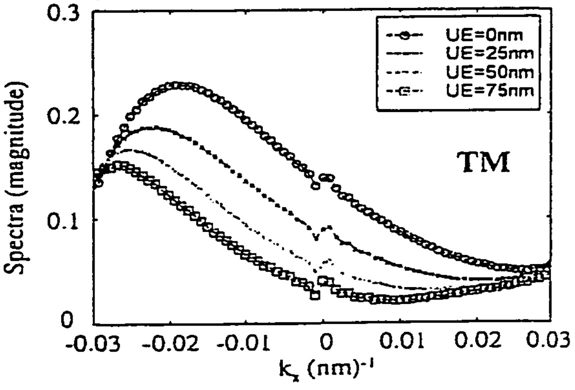

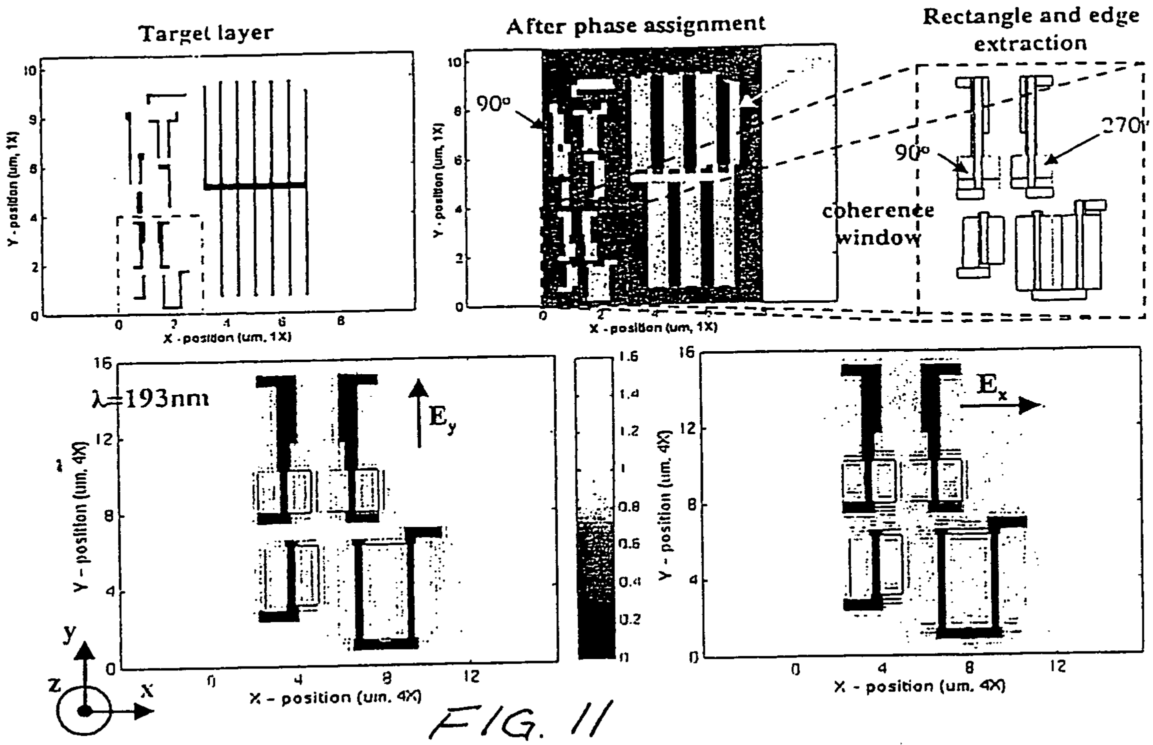

F/G. 11

F/G. 12 (a)

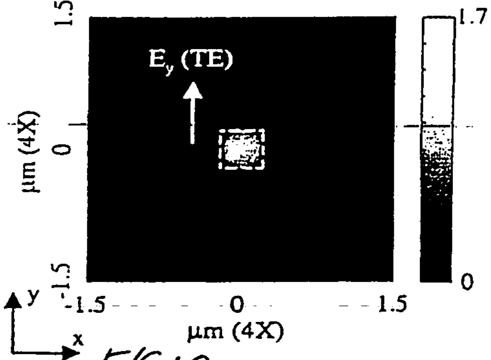

F/G. 12 (b)

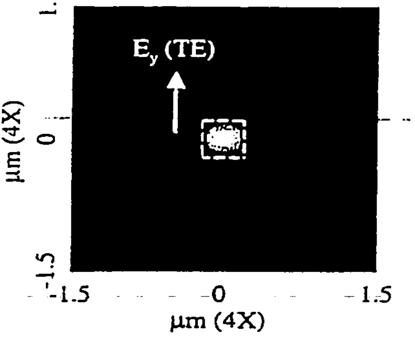

F/G. 12 (c)

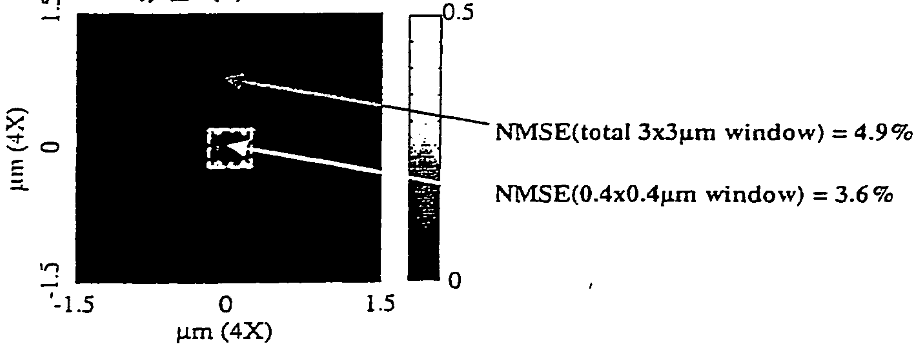

NMSE(total 3x3µm window) = 4.9%

NMSE(0.4x0.4µm window) = 3.6%

FIG. 13 (a)

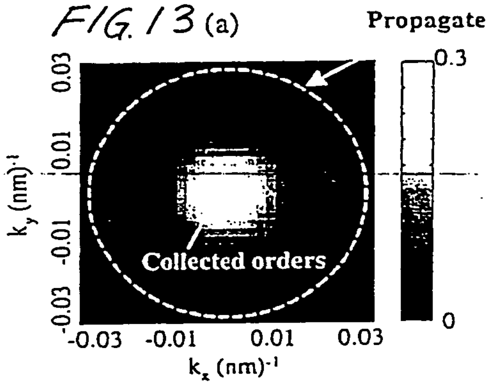

FIG. 13 (b)

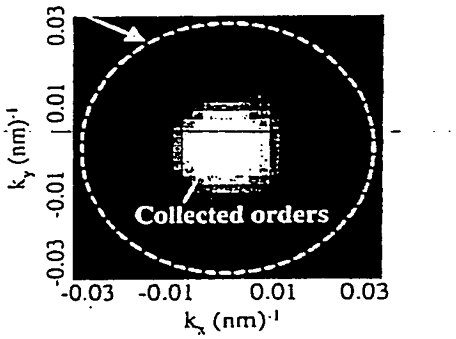

FIG. 13 (c)

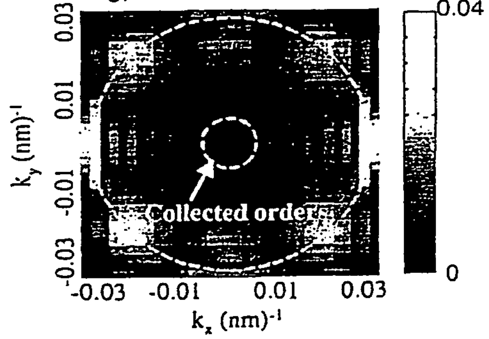

NMSE(propagated orders) = 2.2%

NMSE(collected orders) = 2e-4

FIG. 14 (a)

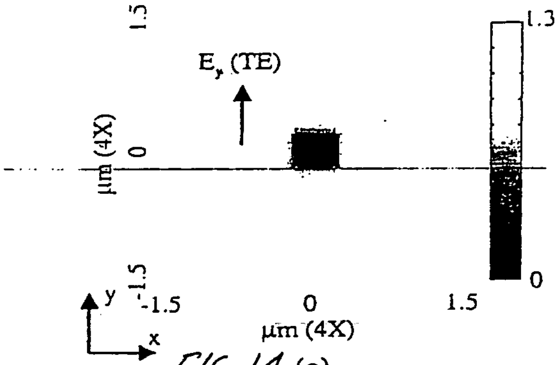

FIG. 14 (b)

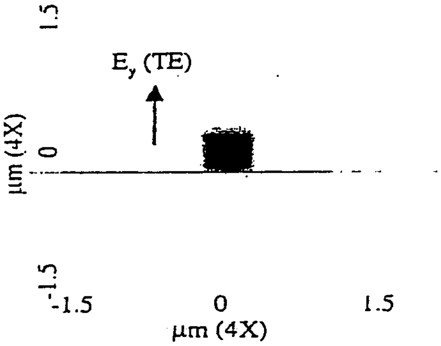

FIG. 14 (c)

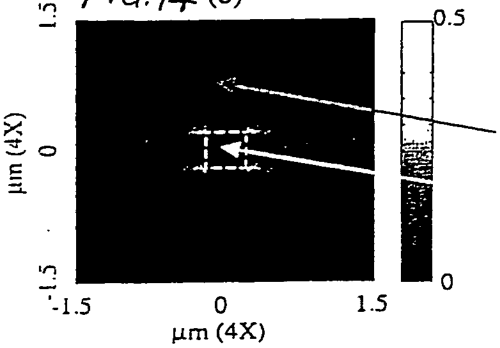

NMSE(total 3x3µm window) = 0.1%

NMSE(0.4x0.4µm window) = 2%

FIG. 15 (a)

Propagated orders

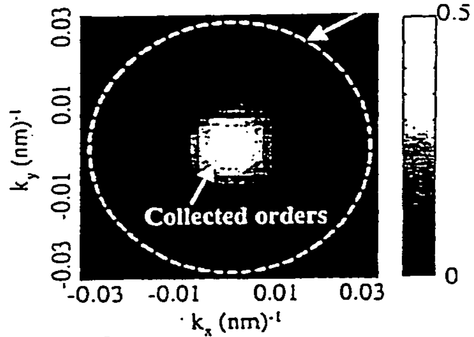

FIG. 15 (b)

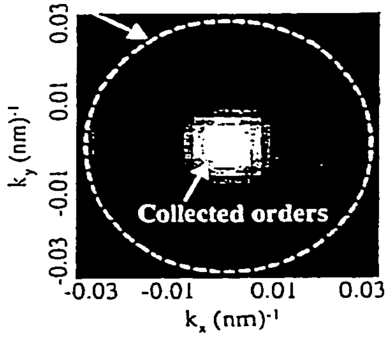

FIG. 15 (c)

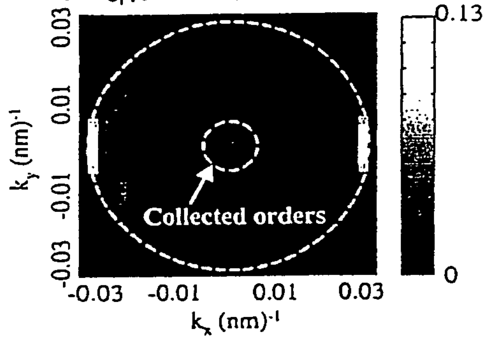

NMSE(propagated orders) = 4%

NMSE(collected orders) = 0.16%

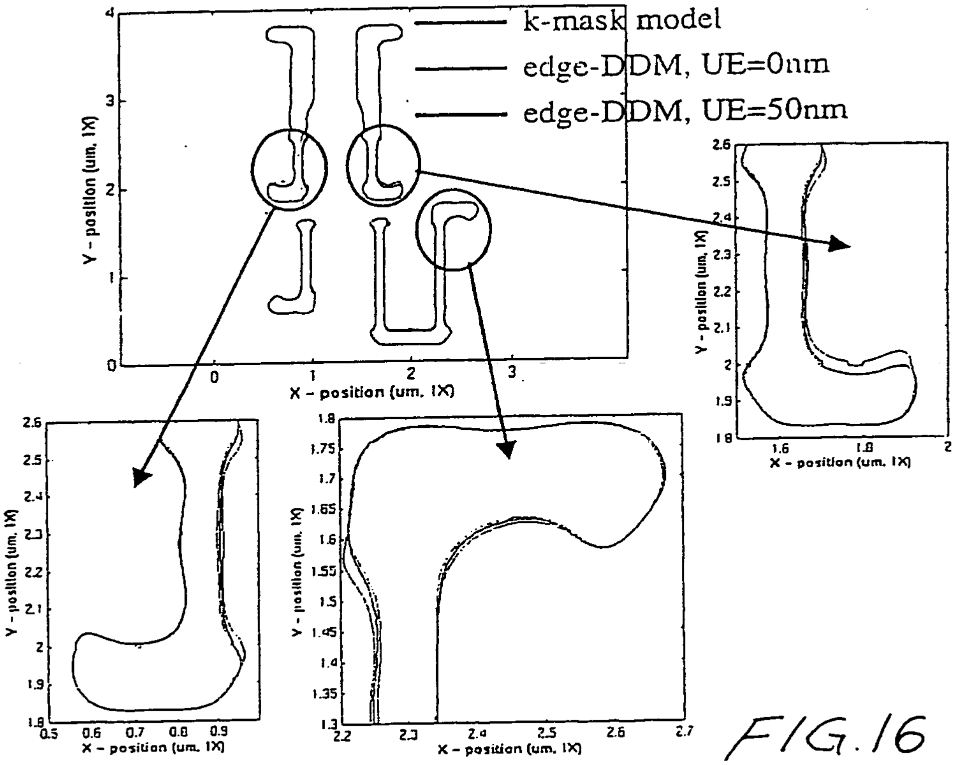

FIG. 16

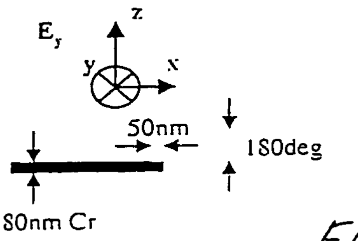

FIG. 17 (a)

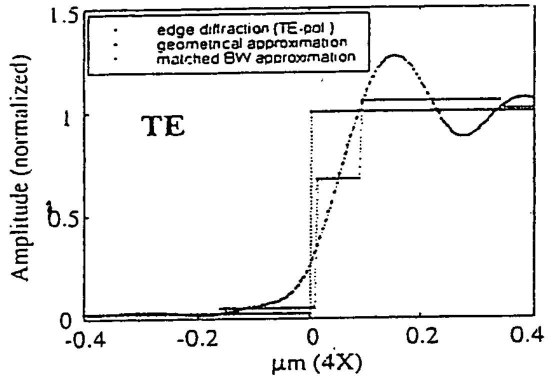

FIG. 17 (b)

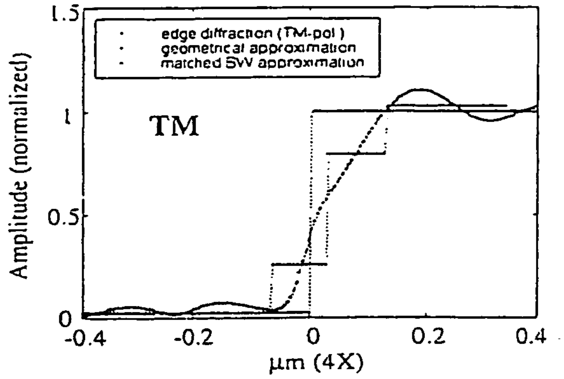

FIG. 18 (a)

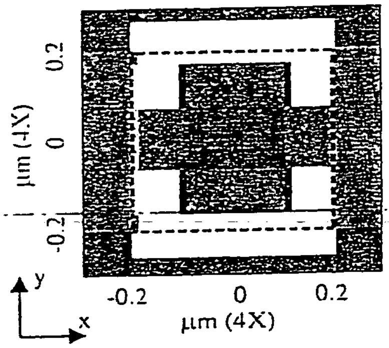

FIG. 18 (b)

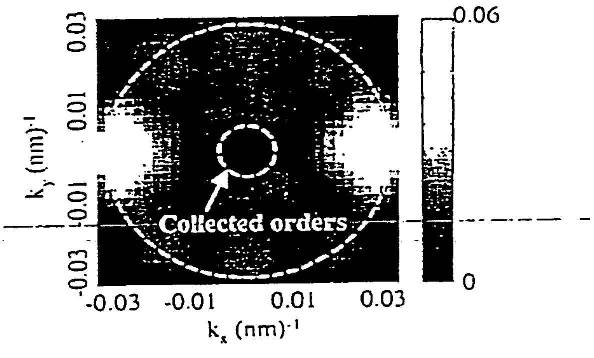

NMSE(propagated orders) = 5.7% (was 2.2%)

NMSE(collected orders) = 8.6e-4 (was 2e-4)

FIG. 19 (a)

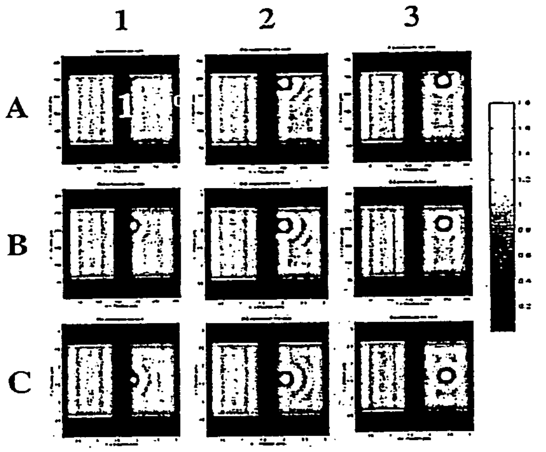

FIG. 19 (b)

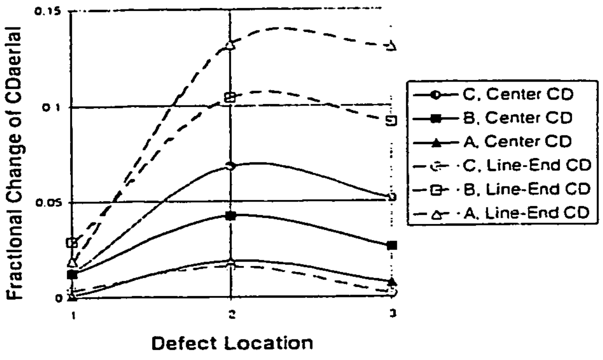

Defect printability assessment (the laborious way)

A square 120nm x 120nm phase defect (post) with 180° height causes different CD variations depending on its relative location with respect to the center line. In general, larger CD variation is evidenced when the defect is close to the line (column 2 in (a)). However, when the defect is partially covered by the Cr-layer of the line, smaller CD changes are observed. This is quantified in (b). The imaging system parameters are: $\lambda=193$nm, NA=0.75, R=4, $\sigma=0.3$. Note that each simulation in (a) requires ~10hrs on a 450MHz CPU.

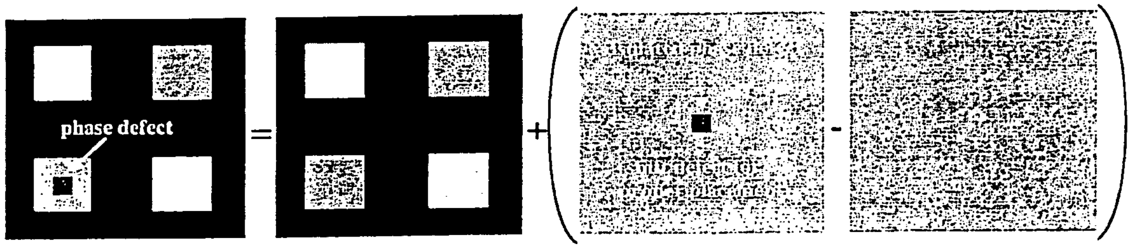

FIG. 20 Domain decomposition method when a defect is present

FIG. 21 (a)

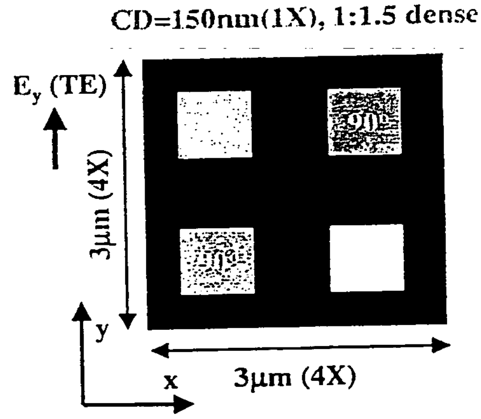

FIG. 21 (b)

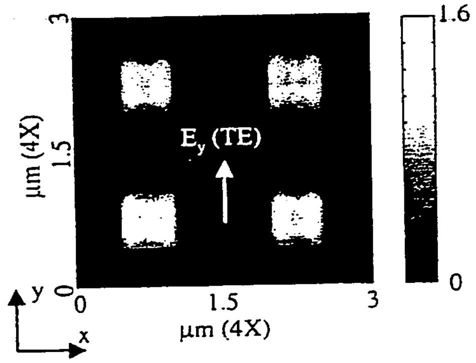

Example: 150nm (1X), 1:1.5 semi-dense, 90°/270° alt. PSM contact mask

(a) Layout and (b) amplitude of scattered field below the mask at the observation plane.

FIG 22(a)

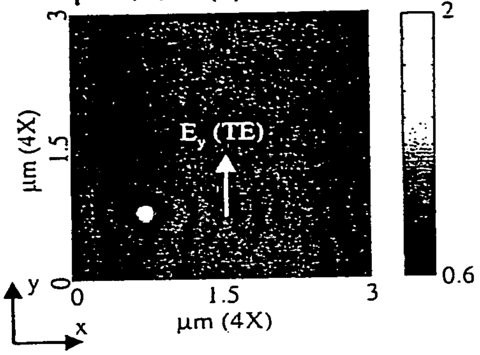

FIG. 22(b)

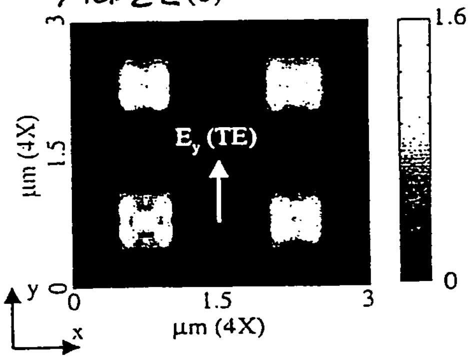

FIG. 22(c)

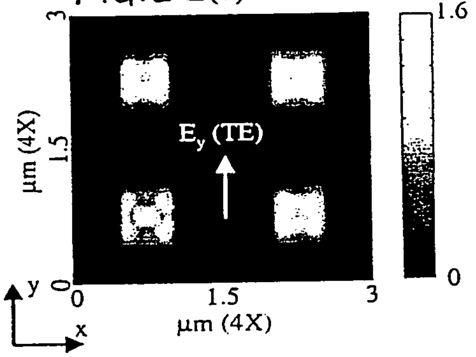

FIG. 22(d)

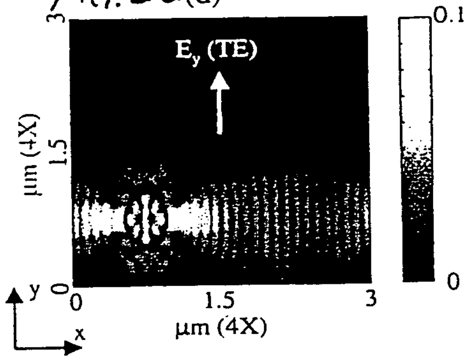

A 90° phase defect present in the center of the bottom-left hole

FIG. 23(a)

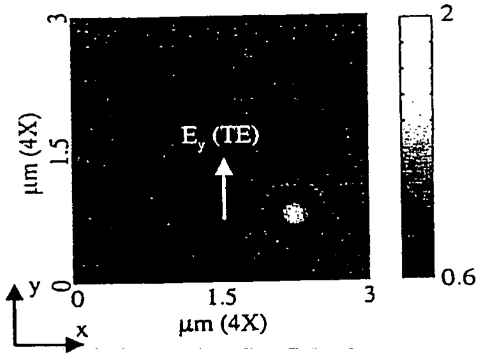

FIG. 23(b)

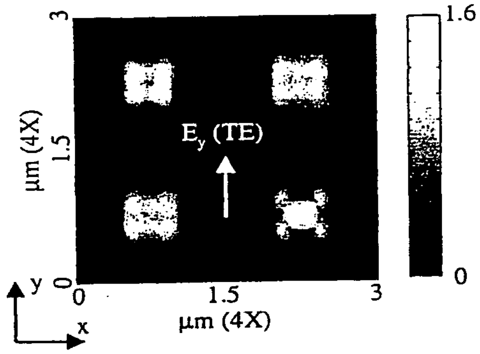

FIG. 23(c)

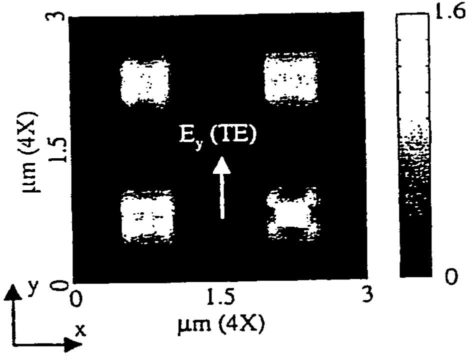

FIG. 23(d)

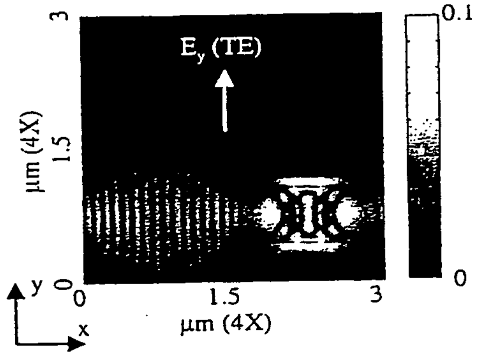

A 90° phase defect present in the center of the bottom-right hole

FIG. 24 (a)

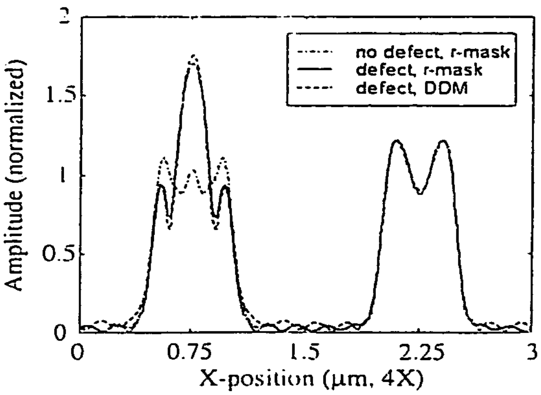

FIG. 24 (b)

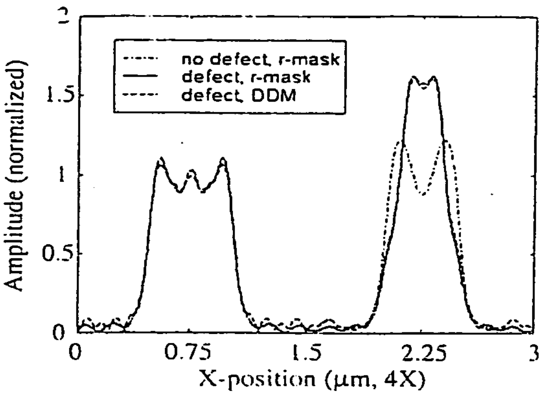

Comparison of the decomposition method with the rigorous solution

(a) Phase defect in the 90° hole and (b) phase defect in the 270° hole. The cut-lines are across x, passing through the center of the defective holes.

FIG. 25 (a)

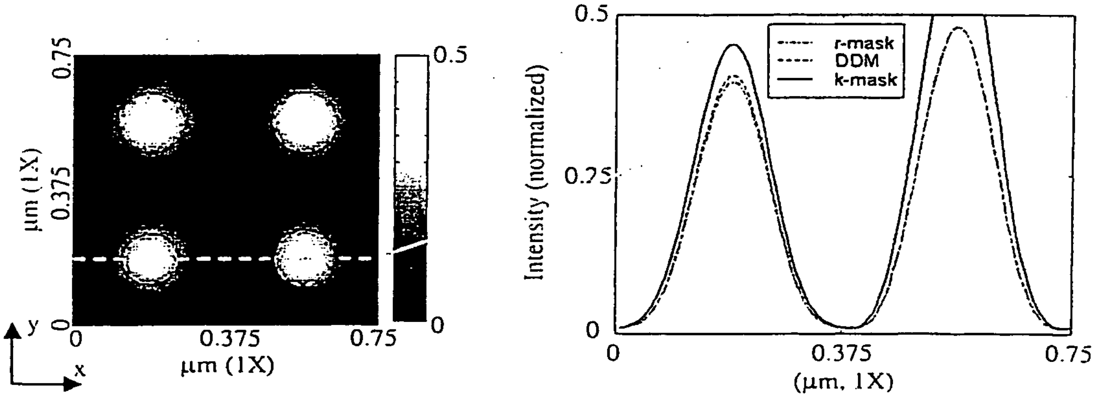

FIG. 25 (b)

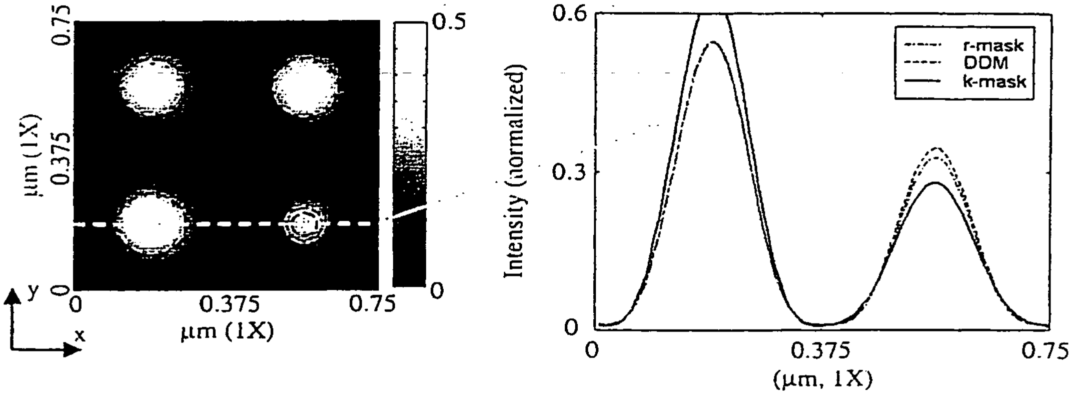

Aerial images of defective masks of Figure 22 and Figure 23

(a) Phase defect in the 90° hole (bottom-left) and (b) phase defect in the 270° hole (bottom-right). Imaging system parameters λ=193nm, R=4, NA=0.75, σ=0.3.

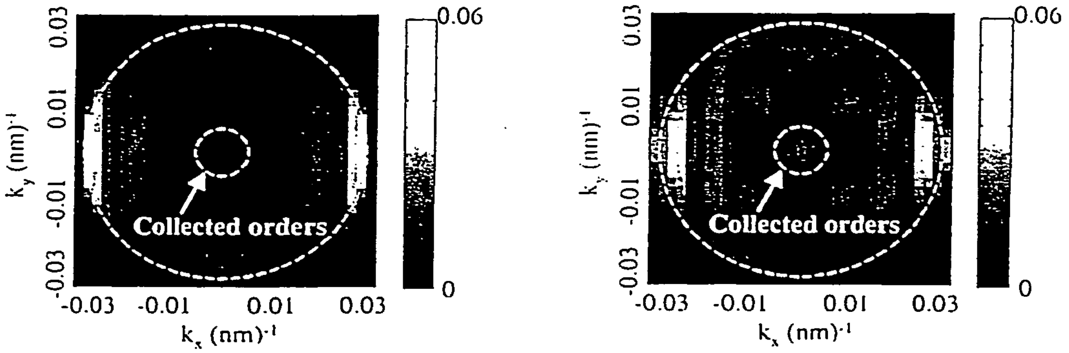

FIG. 26 (a)

FIG. 26 (b)

Spectra plots (magnitude) of the errors of Figure 22 (d) and Figure 23 (d)

- The error is concentrated at the extremities of the spectrum of propagating plane waves indicated by the outer circle and does not exceed 6%. However, the projection printing system (with λ=193nm, R=4, NA=0.75, σ=0.3) uses only the diffraction orders indicated by the inner circle, where the error levels are minimal.